Earth and Planetary Science Letters 579 (2022) 117366

Contents lists available at ScienceDirect

Earth and Planetary Science Letters

www.elsevier.com/locate/epsl

Machine learning bridges microslips and slip avalanches of sheared granular gouges

Gang Ma [a,b], Jiangzhou Mei [a,b,*], Ke Gao [c], Jidong Zhao [d], Wei Zhou [a,b], Di Wang [a,b,e]

[a] State Key Laboratory of Water Resources and Hydropower Engineering Science, Wuhan University, Wuhan 430072, China
[b] Key Laboratory of Rock Mechanics in Hydraulic Structural Engineering of Ministry of Education, Wuhan University, Wuhan 430072, China
[c] Department of Earth and Space Sciences, Southern University of Science and Technology, Shenzhen 518055, Guangdong, China
[d] Department of Civil and Environmental Engineering, The Hong Kong University of Science and Technology, Clear Water Bay, Kowloon, Hong Kong, China
[e] State Key Laboratory of Geomechanics and Geotechnical Engineering, Chinese Academy of Sciences, Wuhan 430071, China

ARTICLE INFO

Article history:
Received 21 July 2021
Received in revised form 25 November 2021
Accepted 3 January 2022
Available online 12 January 2022
Editor: R. Bendick

Keywords:
granular fault gouge
stick slip
microslip
stress drop
spatial correlation

ABSTRACT

Understanding the origin of stress drop of fault gouges may offer deeper insights into many geophysical processes such as earthquakes. Microslips of sheared granular gouges were found to be precursors of large slip events, but the documented relation between microslips and macroscopic stress drops remains largely qualitative. This study aims to quantitatively connect microslips to macroscopic stress fluctuations, including both stress recharges and stress drops. We examine the stick-slip behavior of a slowly sheared granular system using discrete element method simulations. The microslips are found to demonstrate significantly different statistical and spatial characteristics between the stick and slip stages. We further investigate the correlation between the macroscopic stress fluctuations and the features extracted from microslips based on a machine learning (ML) approach. The data-driven model that incorporates the information of the spatial distribution of microslips can robustly predict the magnitude of stress fluctuation. A further feature importance analysis confirms that the spatial patterns of microslips manifest key information governing the macroscopic stress fluctuations. The generalization of ML across granular gouges with different characteristics indicates the proposed model can be applicable to a broad range of granular materials. Our findings in this study may shed lights on the mechanisms governing earthquake nucleation, microslips, friction fluctuations, and their connection during the stick-slip dynamics of earthquake cycles.

1. Introduction

The frictional stability of fault gouge layers underpins key understandings to many geophysical processes, including but not limited to earthquakes, debris flows, and landslides (Song et al., 2017; Ren et al., 2019). A granular gouge subjected to slow shearing demonstrates a typical stick-slip behavior, which plays a crucial role in triggering the frictional stability of the fault (Marone, 1998; Aharonov and Sparks, 2004; Dorostkar and Carmeliet, 2019). Therefore, the stick-slip behavior of sheared granular gouges has been studied extensively in both laboratory experiments (Marone, 1998; Niemeijer et al., 2010; Scuderi et al., 2016; Rivière et al., 2018) and computer simulations (Aharonov and Sparks, 2004; Mair & Hazzard, 2002; Ferdowsi et al., 2014; Gao et al., 2018; Ma et al., 2020). Particular attention has been placed on the influences of controlling factors on the stick-slip dynamics of granular gouges, such as the wall geometry and friction (Rathbun et al., 2013), presence of liquids (Dorostkar et al., 2018), particle characteristics (Mair et al., 2002; Dorostkar and Carmeliet, 2019), boundary vibration (Ferdowsi et al., 2014), normal pressure (Gao et al., 2018), particle size polydispersity (Ma et al., 2020), and particle breakage (Wang et al., 2021). These studies offer novel insights into the complex dynamic behaviors of natural fault gouges and earthquake physics.

The mechanical response of granular materials is characterized by a series of slip avalanches alternating slow elastic loading and rapid sliding and relaxation, leading to jerky dynamics and stress drops (Houdoux et al., 2021). However, the microscopic origin of slip avalanche of slowly deformed granular gouge remains poorly understood. To address this issue, Johnson et al. (2013) employed a biaxial shear apparatus to investigate the physics of laboratory earthquakes and found that the acoustic emission and microslip exhibit an exponential increase in the rate of occurrence, reach-

* Corresponding author at: State Key Laboratory of Water Resources and Hydropower Engineering Science, Wuhan University, Wuhan 430072, China.
E-mail address: whu_meijz@whu.edu.cn (J. Mei).

https://doi.org/10.1016/j.epsl.2022.117366
0012-821X/

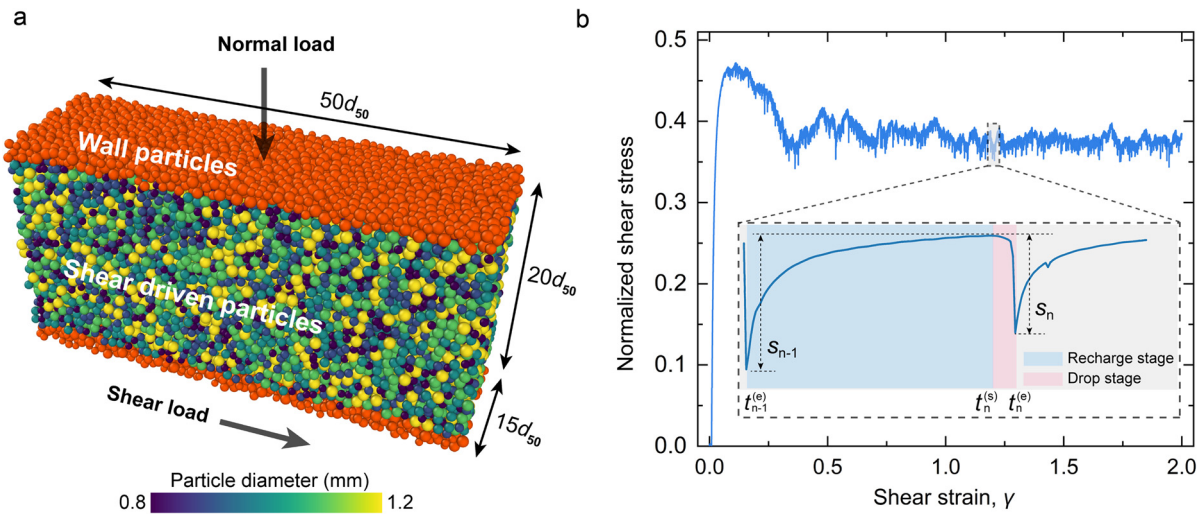

Fig. 1. (a) Setup of the DEM experiment. Normal pressure and shear displacement are respectively applied on the top and bottom particle walls. Periodic boundary conditions are applied in the shear and depth directions. (b) Stress-strain curve resulted from the DEM simulation. The y axis denotes the shear stress σ normalized by the normal pressure p. The inset shows an enlarged stick-slip cycle which consists of stress recharge and drop stage represented by the blue and red shaded region, respectively. (For interpretation of the colors in the figure(s), the reader is referred to the web version of this article.)

ing a peak at the onset of slip avalanche. The corresponding DEM simulations confirmed that the microslip event rate correlates well with large slip event onset (Ferdowsi et al., 2013). Microslip is essentially a result of localized particle rearrangements (Ma et al., 2021). Due to the disordered structure of granular materials, a microslip may trigger nearby microslips, and the accumulation of these microslips may give rise to a macroscopic stress drop (Cao et al., 2019). Thus, microslips are widely regarded as precursors of large slip events and can be used to predict frictional weakening (Bolton et al., 2020; Trugman et al., 2020).

Furthermore, the statistics of microslips and macroscopic stress drops reveal a simple relation between the number of microslips and the stress drops (Barés et al., 2017). The spatial characteristics of microslips are also closely correlated with the stress drop, where large stress drop is accompanied by a series of connected localized zones spanning the entire system, whereas during the elastic regime, the microslip events occur with low concentration and are spatially dispersed (Cao et al., 2018). Other particle scale metrics, such as coordination number, sliding contact ratio, potential energy, kinetic energy, evolves correspondingly during the stick phase and slip instability (Barés et al., 2017; Ma et al., 2020). Thus, studying the microscopic structure and dynamics of a granular gouge may help unveil its stick-slip behaviors (Cipelletti et al., 2019).

Unfortunately, existing findings on the relation between microslips and macroscopic stress drop remains largely qualitative, whereas further advance on the subject matter demands quantitative correlations to be established. In this study, we employ a machine learning (ML) approach to quantitatively bridge microslips and macroscopic stress fluctuations, including both stress recharge (stick regime) and stress drop (slip regime). The stress fluctuation is defined as the change of shear stress at the start and end of the recharge/drop stages. ML offers data-driven approaches to automatically investigate the underlying relations between variables and facilitate the process of revealing complex and inexplicit patterns of large datasets (Marone, 2018). Particularly, ML has gained increasing popularity in recent years and has been widely used in many areas of geoscience, such as predicting the timing and size of laboratory earthquakes (Rouet-Leduc et al., 2017; Corbi et al., 2019), revealing the frictional state of granular fault (Ren et al., 2019), estimating earthquake magnitude and GPS displacement rate (Rouet-Leduc et al., 2019; Mousavi and Beroza, 2020), and performing earthquake early warning and earthquake detection (Hulbert et al., 2019; Trugman et al., 2020).

To do so, we perform the discrete element method (DEM) simulations of quasi-static shear of a granular gouge to achieve stick-slip dynamics. The microslips are manifested as particle rearrangements and quantified by nonaffine particle motions. Then we compare the statistical and spatial characteristics of microslips in the stick and slip regimes. We use a two-step scheme for feature selection to consider both the statistical and spatial characteristics of microslips in the ML model training. The trained ML model can well predict the macroscopic stress fluctuation from the features extracted from the microslips. Finally, we analyze the feature importance of the trained ML model and conclude that the spatial patterns of microslips contain key information about the stick-slip dynamics of the granular gouge.

2. Materials and methods

2.1. DEM simulation of simple shear

DEM simulations of simple shear tests were performed to obtained data of microslips and macroscopic stress fluctuations during the stick-slip cycles of granular gouges. Fig. 1a shows the simple shear model setup of the granular gouge, which consists of 20,215 particles with diameters uniformly distributed from $0.8d_{50}$ to $1.2d_{50}$, where the average particle diameter $d_{50} = 1.0$ mm. The size of the granular gouge sample is $50d_{50}$ (length) $\times$ $15d_{50}$ (depth) $\times$ $20d_{50}$ (height). The granular gouge is confined by two rough particle walls used to apply the shear loading and normal pressure. The top wall is fixed in the shear direction, while the normal pressure is maintained constant by a servo-control at 10 MPa. The granular gouge is sheared by moving the bottom wall in the x direction with a constant velocity while the vertical movement is constrained. The shear rate $\dot{\gamma}$, defined as the ratio of shear velocity to the undeformed sample height, is set to 0.1 to achieve stick-slip dynamics.

The numerical simulation is performed by the DEM code LIGGGHTS (Kloss et al., 2012). The Hertz-Mindlin contact model with Coulomb sliding friction is employed to simulate the contacts and deformation between particles. The particles have a density of 2900 kg/m^3, a Poisson's ratio of 0.25, Young's modulus of 65 GPa, a friction coefficient of 0.5, and a restitution coefficient of

0.87 (Ma et al., 2020). The wall particles adopt the same material properties as those in the shear body. The friction coefficient between the particle walls and the shear body is set to 0.9 to enhance surface friction. To collect enough data for the subsequent machine learning, we shear the granular gouge up to a shear strain of 2. The evolution of normalized shear stress, defined as the ratio of shear stress σ to the applied normal pressure p, is shown in Fig. 1b. When it is sheared into the steady-state regime, the gouge is found to undergo typical intermittent dynamics and serrated plastic flow. This phenomenon is seen to be universal in many amorphous solids like metal glasses (Cao et al., 2018), and porous materials (Baró et al., 2013).

The enlarged view of the dotted box shown in Fig. 1b demonstrates that each stick-slip cycle starts with a nonlinear recharge of shear stress and is followed by a rapid drop. The recharge and drop of shear stress correspond to the stick and slip stages, respectively. We define stress fluctuation as the change of shear stress at the start and end of the recharge/drop events. Thus, the stress fluctuation of a drop event is positive, and the recharge event negative. Only the magnitude of stress fluctuation greater than a threshold of 10^{-5} is considered. During the slow shearing of granular gouge, we recorded 4,232 stress drop and recharge cycles.

2.2. Characterization of microslip

Due to the disordered nature and varying local structure of granular gouge, the displacements of particles show a localized and nonaffine pattern. The microslips that occurred during the recharge and drop events are manifested as irreversible particle rearrangements which are hereby quantified by the nonaffine particle displacements $D^2_{\min}$ (Ma et al., 2021). It should be noted that many other quantities, such as local displacement, local energy fluctuation (Barés et al., 2017; Zheng et al., 2018), granular temperature (Ma et al., 2019), local acoustic emission (Trugman et al., 2020), force chain bulking (Gao et al., 2019) can also be used for characterizing microplasticity. Here we use the squared nonaffine displacements D^2_{min}, which describes the deviation of a particle's position from the best fit affine transformation of its neighborhood. The nonaffine displacement D^2_{min} over a given stage with the strain $\Delta\gamma$ is calculated as (Chikkadi and Schall, 2012; Cao et al., 2019):

$$D^2_{\min}(\gamma,\Delta\gamma)=\frac{1}{N_i}\sum_{j}^{N_i}\left\{\mathbf{r}_j(\gamma+\Delta\gamma/2)-\mathbf{r}_i(\gamma+\Delta\gamma/2)-\Psi\left[\mathbf{r}_j(\gamma-\Delta\gamma/2)-\mathbf{r}_i(\gamma-\Delta\gamma/2)\right]\right\}^2 \quad (1)$$

where γ denotes the macroscopic shear strain of a given time, the subscript i denotes the designated particle, N_i denotes the number of neighbors of the reference particle, and the index j iterates over the neighbors of the reference particle. A larger D^2_{min} denotes a larger microslip. Ψ is the best fit affine transformation tensor that minimizes the quantity D^2_{min} and can be calculated as:

$$\mathbf{X}=\sum_{j}^{N_i}\left[\mathbf{r}_j(\gamma+\Delta\gamma/2)-\mathbf{r}_i(\gamma+\Delta\gamma/2)\right]\otimes\left[\mathbf{r}_j(\gamma-\Delta\gamma/2)-\mathbf{r}_i(\gamma-\Delta\gamma/2)\right] \quad (2)$$

$$\mathbf{Y}=\sum_{j}^{N_i}\left[\mathbf{r}_j(\gamma-\Delta\gamma/2)-\mathbf{r}_i(\gamma-\Delta\gamma/2)\right]\otimes\left[\mathbf{r}_j(\gamma-\Delta\gamma/2)-\mathbf{r}_i(\gamma-\Delta\gamma/2)\right] \quad (3)$$

$$\Psi=\mathbf{X}\cdot\mathbf{Y}^{-1} \quad (4)$$

The spatial correlation of microslips that occurred during the recharge or drop stage can be quantified using the normalized spatial correlation function (Ma et al., 2019, 2021):

$$C_{D^2_{\min}}(r)=\frac{\left\langle D^2_{\min}(0)D^2_{\min}(r)\right\rangle-\left\langle D^2_{\min}\right\rangle^2}{\left\langle\left[D^2_{\min}\right]^2\right\rangle-\left\langle D^2_{\min}\right\rangle^2} \quad (5)$$

where the brackets denote averaging over all particles. The normalized spatial correlation function represents the spatial similarity of $D^2_{\min}$ between two particles separated by the distance r. A larger value corresponding to a stronger correlation over space.

The spatial correlation of microslips can also be quantified by global Moran's I:

$$I=\frac{N}{\sum_i\sum_j w_{ij}}\times\frac{\sum_{i=1}^{N}\sum_{j=1}^{N}w_{ij}\left(D^2_{\min,i}-\left\langle D^2_{\min}\right\rangle\right)\left(D^2_{\min,j}-\left\langle D^2_{\min}\right\rangle\right)}{\sum_{i=1}^{N}\left(D^2_{\min,i}-\left\langle D^2_{\min}\right\rangle\right)^2} \quad (6)$$

where N is the number of particles. w_{ij} is the spatial weights matrix. $w_{ij}=1$ for $r_{ij}\le 2.3d_{50}$ (cutoff distance $2.3d_{50}$ defines the second nearest neighborhood shell), otherwise $w_{ij}=0$. Moran's I evaluates whether the pattern expressed is clustered ($0<I\le 1$), dispersed ($-1\le I<0$), or random ($I\approx 0$).

2.3. Introduction to extreme gradient boosting (XGBoost)

In order to establish a quantitative relation between microslips and the magnitude of macroscopic stress fluctuation, we resort to use the Extreme Gradient Boosting (XGBoost) technique to interrogate the data (Chen and Guestrin, 2016). Gradient boosting decision is an extensively used machine learning ensemble method (Friedman, 2002). By changing the weights of training samples, gradient boosting improves the prediction performance by learning multiple simple models and linear combination of these models. XGBoost was introduced as a robust decision tree based on the gradient boosting decision. The methodology of XGBoost is briefly introduced below.

Given the data $\{(\boldsymbol{x}_i, y_i), i=1,2,...m\}$, the decision function of XGBoost which consists of K additive functions can be expressed as:

$$\hat{y}_i=f(\boldsymbol{x}_i)=\sum_{k=1}^{K}f_k(\boldsymbol{x}_i) \quad (7)$$

where $\boldsymbol{x}_i$ is the vector of the input features and y_i is the corresponding output value. $f_1, f_2, ..., f_k$ is a sequence of classification and regression trees (CARTs). XGBoost uses the additive training strategy. Specifically, the structures of all trees in XGBoost are not determined at the same time. Instead, the tree structure is fixed at each step and then a new tree is added to fit the residual error. f_t is added into the ensemble trees by minimizing the objective function as follows:

$$L^{(t)}=\sum_{i=1}^{m}l\left(y_i,\hat{y}_i^{(t-1)}+f_t(\boldsymbol{x}_i)\right)+\Omega(f_t) \quad (8)$$

where l is the desired loss function which describes the difference between the predicted response value and the actual response value. The commonly used loss function is the Mean Square Error

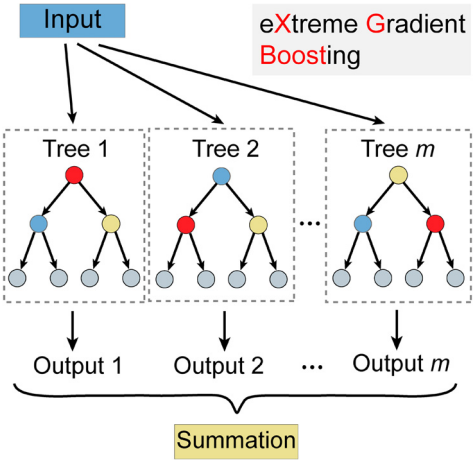

Fig. 2. Schematic of XGBoost (a supervised ML approach) based on the gradient boosting decision.

(MSE). m is the total sample size, y_i is the measured value, $\hat{y}_i^{(t-1)}$ is the i^{th} predicted response at the $(t-1)$ step. Ω is the penalty function to limit the model complexity, which can be described as:

$$\Omega(f) = \gamma T + \frac{1}{2}\lambda \sum_{j=1}^{T} \boldsymbol{w}_j^2 \tag{9}$$

where γ denote the complexity of each leaf, T is the number of leaves in a tree, λ is a penalty parameter, and $\boldsymbol{w}$ denotes the vector of scores on leaves. A typical structure of a XGBoost is depicted in Fig. 2.

The training and validation process of XGBoost is described as follows. The dataset is divided into the training set, validation set, and test set. XGBoost model has several hyperparameters, such as learning rate, maximum depth and number of trees. The validation set is used to evaluate the performance of XGBoost model with different hyperparameter values. However, tuning machine learning models manually can be a very time-consuming task. In this paper, we employ Bayesian Optimization to automatically tune the hyperparameters of XGBoost (Snoek et al., 2012). Bayesian Optimization builds a surrogate for this objective and quantifies the uncertainty in that surrogate using the Gaussian process regression, and then uses an acquisition function to decide the next combination to be tried. Once the optimal set of hyperparameters are determined, we can guarantee the XGBoost model has good generalization performance and prediction accuracy. The test set is finally used to test the prediction performance of the tuned XGBoost.

3. Results

3.1. Statistical and spatial characteristics of microslips

Fig. 3a and 3b show the spatial distributions of $D^2_{\min}$ during the recharge and drop stages of a typical stick-slip cycle. Particles with higher $D^2_{\min}$ are colored in red. Due to the discrete nature and corporative particle motion of granular materials, the deformation of granular assembly occurs as a succession of localized microslips distributed within the system. Intuitively, the microslips are scattered throughout the granular system during the recharge stage. During the drop stage, the microslips are more spatially concentrated and tend to generate a large stress drop inside the granular system. Fig. 3c compares the statistical features of microslips that occurred during the recharge (blue) and drop stages (red). The microslips demonstrate significantly different statistical characteristics at the recharge and drop stages. For example, the 99.5^{th} percentile, max, variance, skewness, and kurtosis are larger for drop stage. The difference in statistics of microslips may suggest different underlying mechanism for stress recharge and stress drop. The stick-slip dynamics of granular materials can be seen as a jamming-unjamming process accompanied by the formation and buckling of force chains, which are triggered by localized particle rearrangements known as microslips (Barés et al., 2017; Gao et al., 2019).

The spatial correlation of microslips that occur during the recharge and drop stage can be further quantified using the normalized spatial correlation function. We group the recharge and drop events according to the magnitude and sign of stress fluctuation. Logarithmic binning is used. Fig. 3d shows the normalized correlation function $C_{D^2_{min}}(r)$ for recharge and drop events of different magnitudes. The spatial autocorrelation decays rapidly within a short distance of several d_{50}, showing a short-range ordering. Solid lines indicate that the decay of correlations with r are reasonably well fitted by the Ornstein-Zernike function as $C_{D^2_{min}}(r) \propto r^{-0.5}\exp(-r/\xi_r)$. We can see that the correlation length of microslips ξ_r remains nearly unchanged for recharge events and increases rapidly for large stress drop (see red line and left axis of Fig. 3e). This trend indicates that a more cooperative and concentrated distribution of microslips constitutes the microscopic origin of global slip avalanche.

The spatial autocorrelation of microslips can also be quantified by global Moran's I. The Moran's I of particle $D^2_{\min}$ for recharge and drop events of different magnitudes show a very similar trend as the correlation length ξ_r (see blue line and right axis of Fig. 3e). The spatial correlation analysis of microslips indicates that the spatially correlated microslips forming large shear transition zones are responsible for the stress drop and frictional weakening. The stress drop increases with the increasing degree of aggregation of microslips. The spatial distribution of microslips during recharge stages shows on average a plateau over different bins.

3.2. Machine learning predicts stress fluctuations

In this paper, we utilize XGBoost to link microslips and macroscopic stress fluctuations, i.e., the input of XGBoost is the statistical features of microslips occurred during a recharge stage or a drop stage, and the output is the corresponding macroscopic stress fluctuation. Thus, the time window over which the microslips are defined and the statistics are computed varies in the dataset. The above analysis demonstrates a clear difference of microslips between recharge and drop events. Therefore, it is necessary to consider both the statistical and spatial characteristics of microslips in the feature extraction. For each particle, we define its medium-range statistics within its neighborhood (see Fig. 4a). Specifically, we calculate the maximum, mean, variance, skewness, and kurtosis of particle $D^2_{\min}$ within each particle's neighborhood. The symbols in Fig. 4 and their meanings are illustrated in Table A1. Thus, each particle is characterized by five medium-range features, containing information about how it moves and the collective motion of neighboring particles. We then calculate the statistical features of each particle's medium-range statistics (see Fig. 4b). The statistical operator includes mean, max, variance, percentiles, and various higher-order moments. These statistical features are connected as the medium-range feature vector (MRF). Thus, the MRF is dependent on the neighborhood size and may influence the ML performance.

To investigate the influence of neighborhood size on the performance of ML, we extract the MRFs with different neighborhood sizes for the downstream ML regression. Fig. 5a shows the pair correlation function $g(r)$ of the granular gouge. Pair correlation function is calculated as $g(r) = \frac{N(r)}{\rho_0 V} \approx \frac{N(r)}{4\pi r^2 \rho_0 \Delta r}$, where $N(r)$ denotes the number of particles in a shell with the thickness of Δr

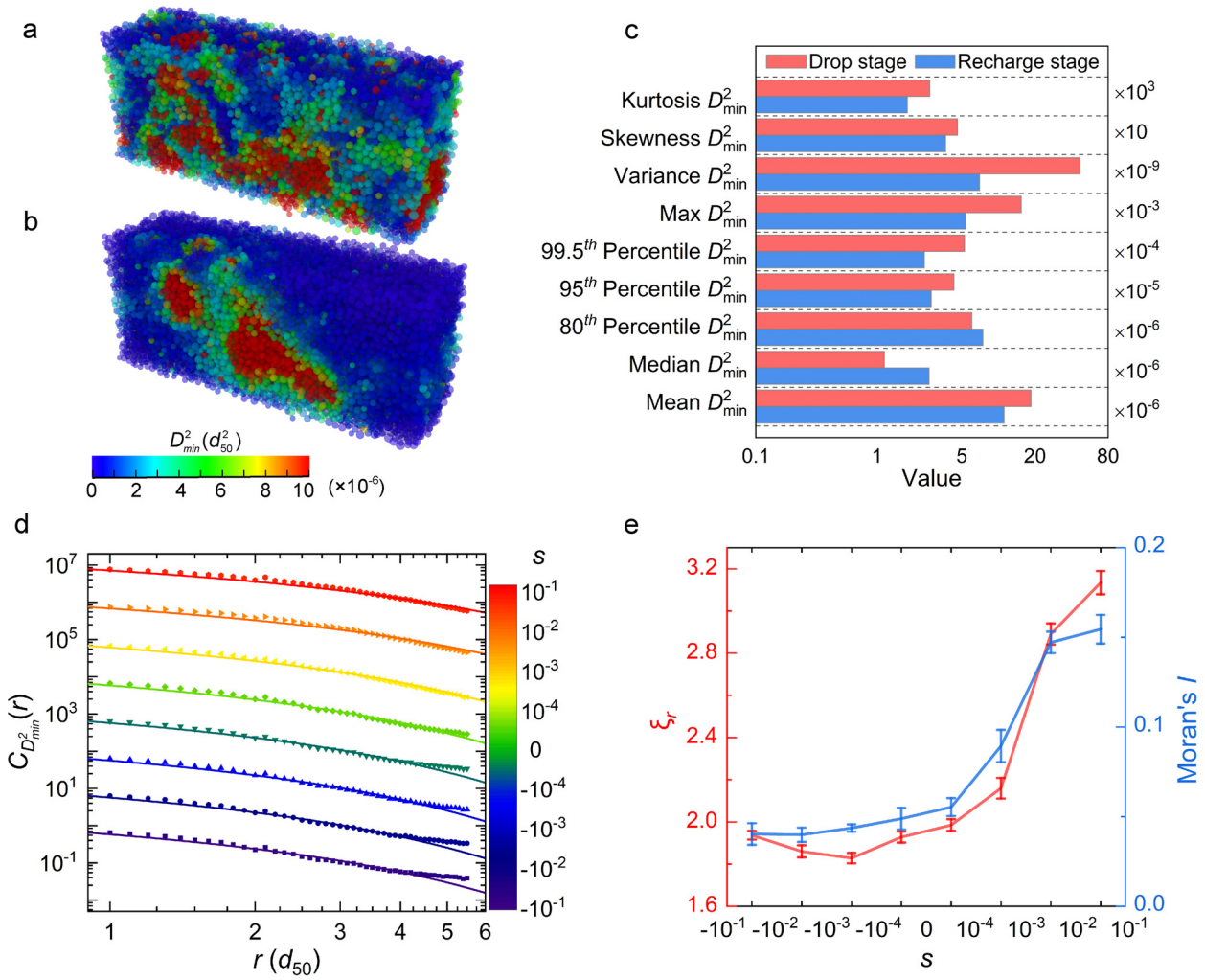

Fig. 3. Statistical and spatial characteristics of microslips occurred during recharge and drop stages. Spatial maps of $D^2_{\min}$ occurred during the (a) recharge stage and (b) drop stage of a typical stick-slip cycle. (c) Comparison of the statistical quantities of $D^2_{\min}$ during the recharge and drop stage. (d) Normalized spatial correlation function of $D^2_{\min}$: $C_{D^2_{min}}(r)$ between two particles separated by distance r, where r is in unit of the mean particle diameter. The data points are averaged over the recharge or drop stages falling into each bin. Solid lines are fits to the Ornstein-Zernike function. The data points and fitting lines of the different bin are shifted vertically for better visualization. (e) Evolutions of correlation length ξ_r and Moran' I with the magnitude of stress fluctuation. The error bar represents the standard deviation. Note that (d) and (e) are calculated over all stick-slip cycles.

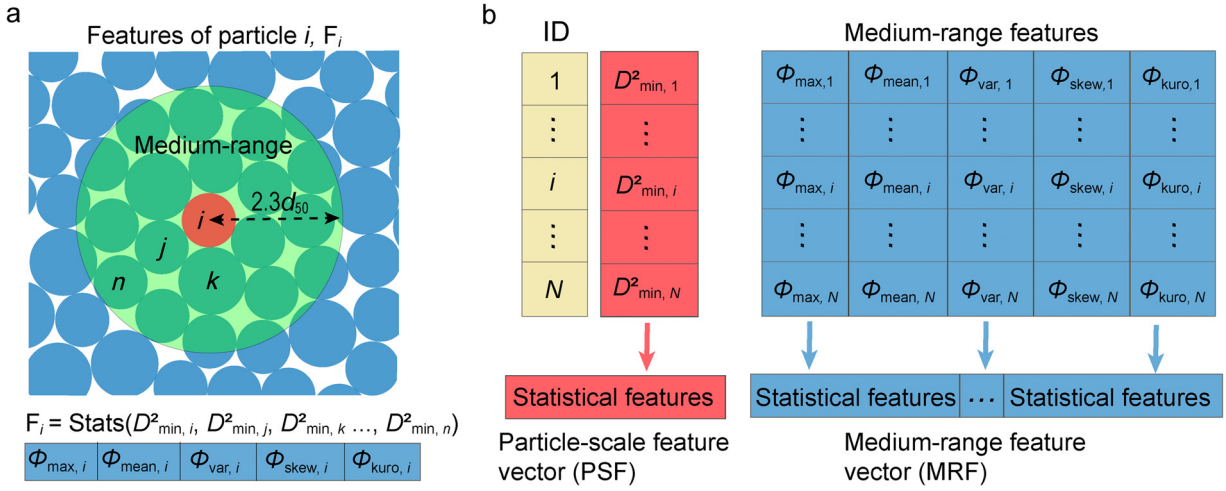

Fig. 4. Machine learning builds the bridge between microslips and macroscopic stress fluctuation. (a) The statistical characteristics of particle $D^2_{\min}$ within each particle's second-neighbor shell. (b) Feature extraction process: particle-scale feature vector (red column) and medium-range feature vector (blue columns). These two feature vectors are fed as input to the downstream XGBoost model to predict macroscopic stress fluctuation.

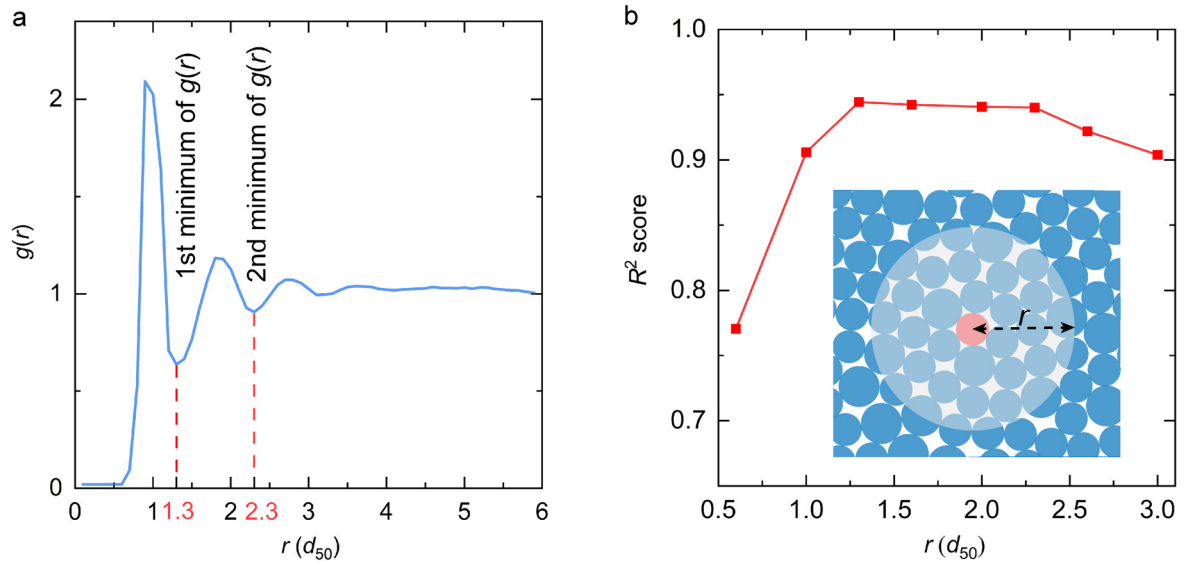

Fig. 5. Evolution of the ML performance with varying neighborhood size. (a) Pair correlation function $g(r)$ of the granular gouge. (b) The ML performance versus different size of particle neighborhood. The inset shows the definition of the neighborhood surrounding the center particle colored by red.

at the distance r from the center particle. ρ_0 is the number density of the granular system. The pair correlation function shows no long-range ordering and periodic peak pattern. The first and second minimum of $g(r)$ corresponding to the first- and second-neighbor shell of a given particle. Fig. 5b shows the variation of ML performance with varying neighborhood sizes. The error bar denotes the standard deviation over 50 independent training and prediction processes. The ML performance in terms of R^2 shows a nonmonotonic behavior. The MRF extracted from the neighborhood between $1.3d_{50}$ and $2.3d_{50}$, corresponding to the first and second minimum of the pair correlation function, gives the best performance. Finally, a neighborhood size of $2.3d_{50}$ is used in this study. Such a short-range characteristic length indicates that the particles are involved in localized structures and the nonaffine motion becomes localized (Ma et al., 2021).

To highlight the importance of the spatial pattern of microslips in the prediction of macroscopic stress fluctuation, we also calculate the statistical features of particles D^2_{min} as the input vector for XGBoost model training. This feature vector does not contain any information about the spatial distribution of microslips, and is referred to as particle-scale feature vector (PSF). MRF and PSF are extracted for each recharge/drop event, and the corresponding output of XGBoost is the macroscopic stress fluctuation of the recharge/drop event.

During the shearing process, a total of 4,232 stick-slip cycles are recorded and used to construct the dataset for XGBoost. Thus, the dataset contains 8,464 samples, and the first 60% is set as the training set, the next 20% as the validation set for the hyperparameters tuning of XGBoost, and the last 20% as the test set for the final evaluation of the tuned XGBoost. These three sets do not overlap each other to avoid "information leakage". The loss function of XGBoost for regression problems is the mean square error (MSE). The hyperparameters of XGBoost are tuned using Bayesian Optimization (Snoek et al., 2012). The performance of XGBoost model using PSF and MRF as inputs are shown in Figs. 6a and 6b, respectively. As can be seen, the trained XGBoost models not only classify the recharge and drop event from the microslips, but also predict the magnitude of stress fluctuation with good accuracy. By taking into account both statistical and spatial characteristics of the microslips, the trained XGBoost model exhibits better performance with a coefficient of determination $R^2 = 0.941$.

3.3. Feature importance analysis

We further analyze the feature importance of the XGBoost model trained by MRF. The feature importance is quantified by Shapley Additive Explanation (SHAP) value (Lundberg and Lee, 2017). The SHAP value for each feature is the average marginal contribution of a feature value across all possible coalitions, representing their contribution towards a higher or lower final prediction. Fig. 7a shows the mean absolute SHAP values of the top 10 important features. The 3^{rd} moment of ϕ_{skew} is the most important feature, which significantly changes the predicted value of stress fluctuation over other features. ϕ_{skew} measures the tail-heaviness of D^2_{min} of a particle's second nearest neighbors (von Hippel, 2005). The closer ϕ_{skew} is to 0, the considered particle and its neighbors move in a more corporative manner, i.e., particles with either high D^2_{min} or low D^2_{min} are spatially clustered.

Fig. 7b shows the frequency distribution of ϕ_{skew} during the recharge stage and drop stages of a stick-slip cycle. The drop stage contains more particles with smaller ϕ_{skew}, resulting in a larger 3^{rd} moment ϕ_{skew}. To investigate how the 3^{rd} moment ϕ_{skew} affects the model prediction, we present the SHAP dependence plot in Fig. 7c. Each dot denotes a recharge/drop event in the ML dataset, and the scatters are colored according to the global Moran's I of particle D^2_{min}. The smaller 3^{rd} moment ϕ_{skew} results in a smaller and negative SHAP value, pushing the XGBoost prediction towards a recharge event. In contrast, microslips of a drop event demonstrate stronger spatial correlation and thus have higher 3^{rd} moment ϕ_{skew}. This feature helps XGBoost to distinguish between the recharge and drop events and predict the magnitude of macroscopic stress fluctuation. This study reveals that the spatial distribution of microslips contains key information on the stress state of a granular system such that microslips (e.g., local acoustic emission signal and local seismic wave) detected inside the natural gouge faults may also be useful to predict its frictional stability.

3.4. Generalization capability of machine learning approach

It should be noted that many particle characteristics, including but not limited to particle shape, size distribution, surface roughness, moisture content, and mineralogy, have been shown to have influences on the frictional instability of granular system (Mair et

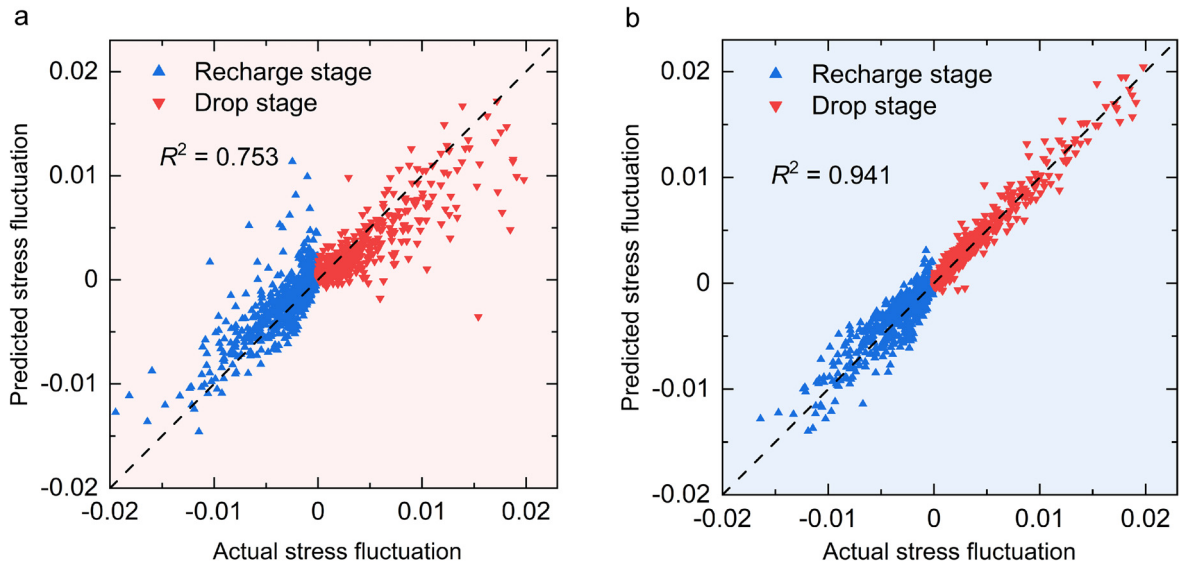

Fig. 6. Performance of XGBoost model trained by (a) PSF and (b) MRF, respectively.

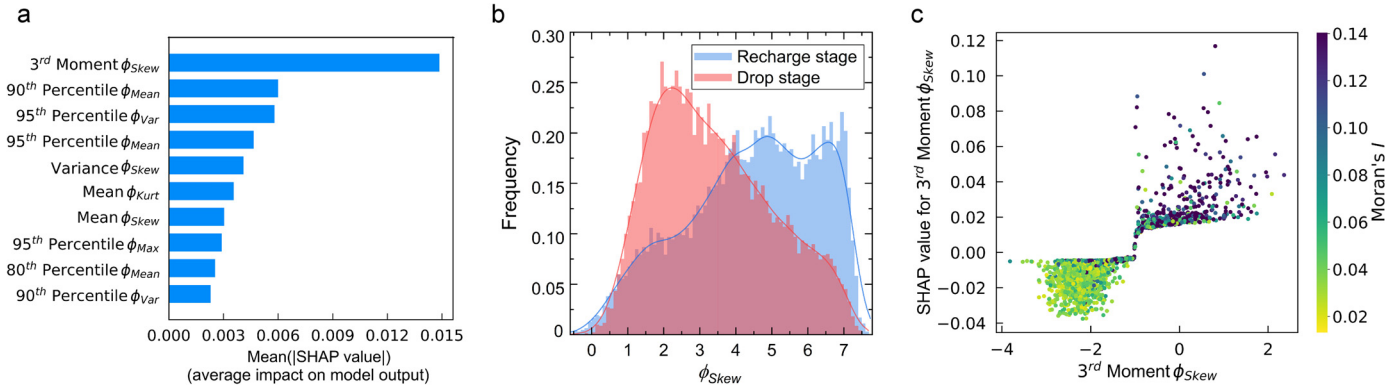

Fig. 7. Feature importance analysis. (a) SHAP values for the top 10 important features. (b) Frequency distributions of ϕ_{skew} during the recharge and drop stages of a stick-slip cycle. The 3^{rd} moment ϕ_{skew} of recharge and drop stage are -2.41 and 1.80, respectively. Solid lines are Kernel Density Estimations used to smooth the distributions. (c) Dependence plot for the 3^{rd} moment of ϕ_{skew}, colored by the global Moran's I.

al., 2002; Anthony and Marone, 2005; Ikari et al., 2011; Scuderi et al., 2014). For example, the shearing of non-spherical particle assembly usually shows a distinct shear band, and microslip activities mainly occur within or near this thin layer.

To investigate whether particle shape could influence the main conclusions of this study, we slowly sheared an assembly of ellipsoidal particles using the same simple shear setup as that of the spherical particle assembly. As a simple yet efficient representation of non-spherical particle shape, ellipsoidal particles are often used in the studies of granular materials (Kou et al., 2018; Murphy et al., 2019). As shown in Fig. 8a, the particle assembly consists of 17,764 prolate ellipsoids with an aspect ratio of 1.5. Figs. 8b and 8c show the spatial maps of particle velocity for assemblies of spherical and ellipsoidal particles and their corresponding velocity profiles. Fig. 8d shows the spatial maps of particle nonaffine particle displacements during two stress drops of similar sizes, respectively, for spherical (top) and ellipsoidal (down) particle assemblies. The ellipsoidal granular assembly has a more distinct shear band along the shear direction, as confirmed by the sharp transition of the velocity profile (Fig. 8c). Following the procedures described above, we train the ML model to predict the stress fluctuations from the microslips of ellipsoidal particle assembly. Fig. 8e shows the performance of the ML model trained by MRF. The ML model has a good performance with a coefficient of determination $R^2 = 0.913$, which indicates that the connection of microslips with macroscopic stress fluctuations using ML model is still valid for non-spherical granular systems.

To further demonstrate the applicability of the proposed approach, we performed several DEM simple shear simulations of granular gouges with different particle size distributions and particle friction coefficients. Four particle size distributions are considered, i.e., particle diameters uniformly distributed on the interval 0.8-1.2d_{50}, 0.9-1.1d_{50}, 0.7-1.3d_{50}, and 0.3-1.7d_{50}. The first one is used in the main text, and the latter three are added here. Three levels of particle friction coefficients are considered, i.e., 0.1, 0.5, and 0.9.

Fig. 9a and 10a show the stress-strain curves of granular gouges with different particle size distributions and particle friction coefficients, respectively. The curves have been shifted vertically to facilitate visual inspection. Fig. 9b to 9d and Fig. 10b to 10d demonstrate the performance of ML methods on these granular gouges. Except for the granular gouge with particle friction coefficient of 0.1, other ML models have R-Squared values higher than 0.9. Together with the case of ellipsoidal particle assembly, we can conclude that the proposed ML approach to connect particle scale

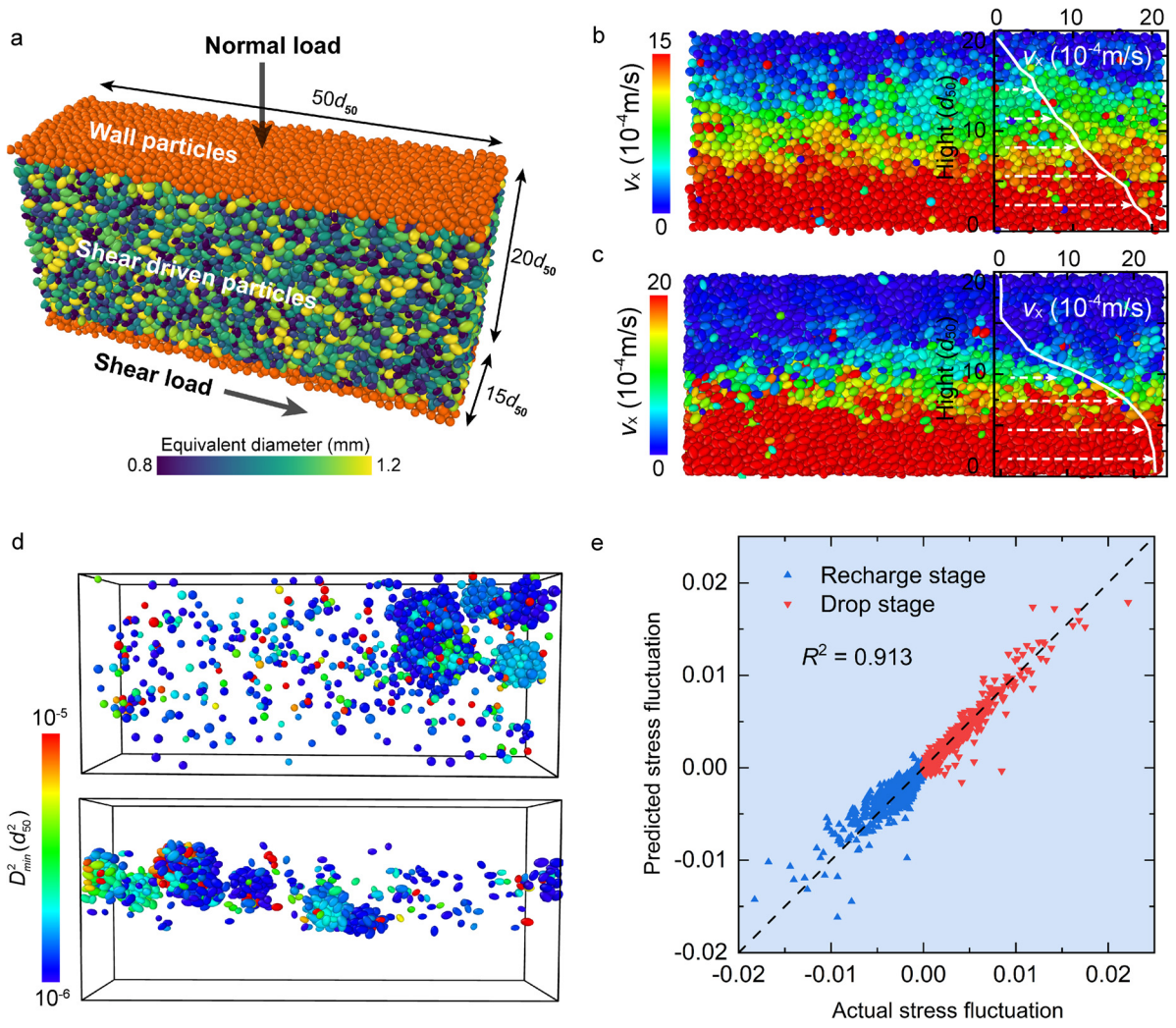

Fig. 8. (a) Simple shear of an assembly of ellipsoidal particles. Normal pressure and shear displacement are respectively applied on the top and bottom particle walls. Periodic boundary conditions are applied in the shear and depth directions. Spatial maps of particle velocity for assemblies of (b) spherical and (c) ellipsoidal particles and their corresponding velocity profiles. (d) Spatial maps of nonaffine particle displacements particle nonaffine displacements during two stress drops of similar sizes, respectively, for spherical (top) and ellipsoidal (down) particle assemblies. (e) Performance of XGBoost model trained by MRF of the ellipsoidal particle assembly.

microslips and macroscopic stress fluctuations is applicable to a broad range of granular materials.

4. Discussion

It is worth mentioning that the microslips are manifested as particle rearrangements and quantified by nonaffine particle motions. Compared to other common interpretations of microslips, such as acoustic emission, emitted seismic waves and shear failures, this particle-scale measure provides a novel approach to quantitatively analyze the statistical properties, spatial characteristics of microslips and their relationship with macroscopic stress drops. However, such approach is not without limitations. The characterization of microslips using particle nonaffine displacements is limited in computer simulations or experiments with x-ray tomography (Xing et al., 2021), light scattering (Le Bouil et al., 2014), etc. Therefore, there is still a long way before we could apply the proposed ML approach to natural fault gouges.

Previous studies have revealed that particle rearrangements and far field acoustic signal are different aspects of the force chain dynamics (Gao et al., 2019; Ma et al., 2021; Tordesillas et al., 2016). The spatial analysis carried in this study can facilitate future understanding into the acoustic emission process in natural fault gouges. With the rapid development of reliable geophysical monitoring, we believe the spatial information of local seismic waves inside natural faults may be used to evaluate the frictional stability of faults. Furthermore, many other ways can also be used to extract the spatial patterns of microslips, such as Convolutional Neural Network, Graph Embedding for feature extraction, and complex network analysis.

5. Conclusions

We quantitatively investigate and establish the relations between microslips and macroscopic stress fluctuations of a slowly sheared granular gouge. The microslips are manifested as particle rearrangements and quantified by nonaffine particle motions. The statistical features and spatial distributions of microslips that occurred during the recharge and drop stages of a stick-slip cycle demonstrate apparently different characteristics. Both the Moran's I and the correlation length of particle $D^2_{\min}$ indicate that microslips in drop stages are spatially correlated to form large stress drops and frictional weakening. The differences in the microscopic dynamics of recharge and drop events suggest that we can quantitatively connect the microslips and macroscopic stress fluctuations.

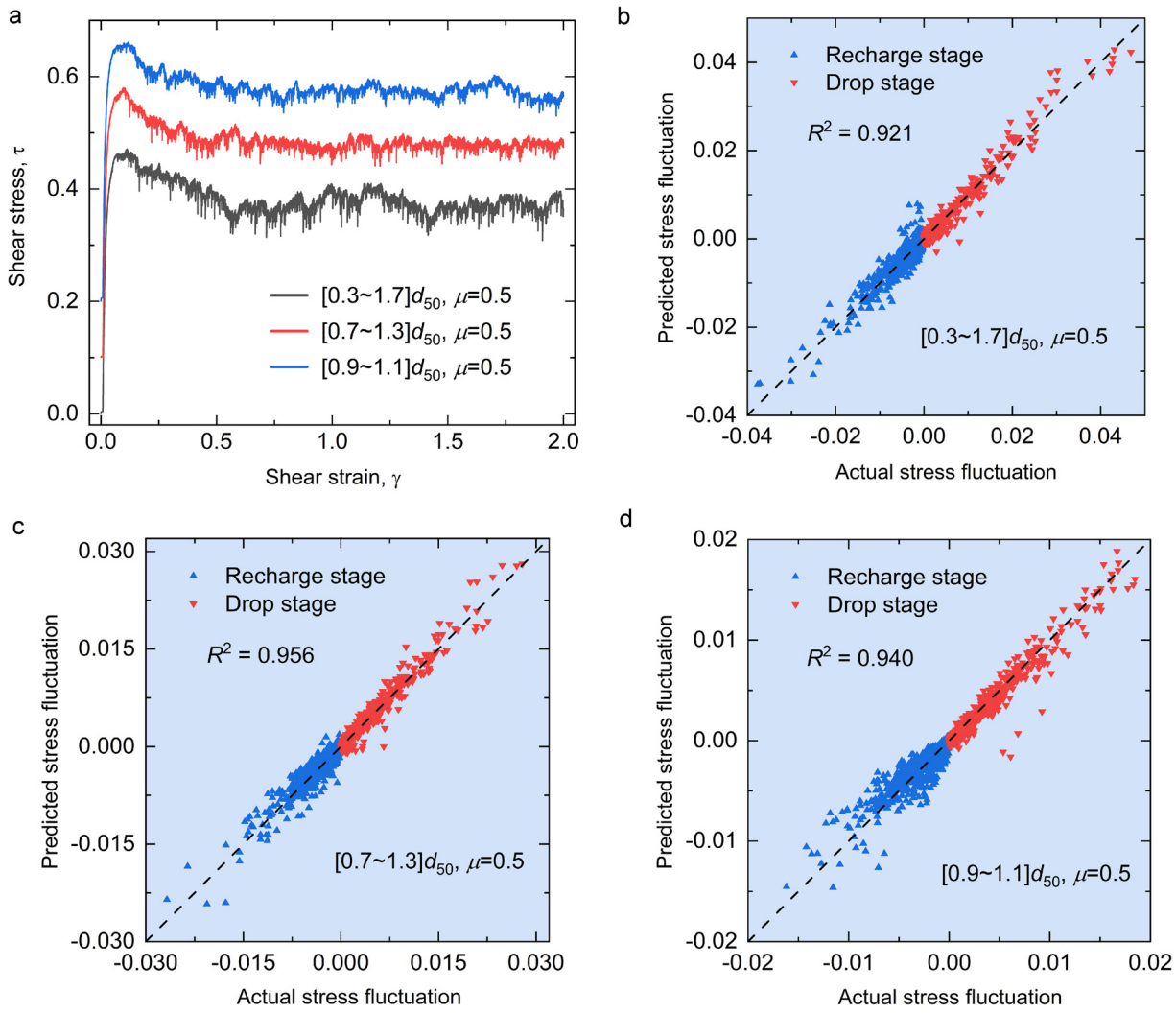

Fig. 9. (a) Stress-strain curves of different size distributions. The two upper curves have been shifted vertically by 0.1, 0.2, respectively, to facilitate visual inspection. The prediction performances of XGBoost trained on these datasets are shown from (b) to (d), respectively. Here we only show the results based on MRF.

The use of XGBoost boosts to build the bridge between microslips and macroscopic stress fluctuation. Two sets of input fractures are extracted from the raw data to train the ML models. By using the input feature vector containing both statistical and spatial information of microslips, the trained XGBoost model can not only distinguish between recharge and drop events but also predict the magnitude of stress fluctuation with good accuracy. The proposed ML approach is applicable to granular gouges with different particle shapes, size distributions, and friction characteristics. The feature importance analysis reveals the feature characterizing the local spatial autocorrelation of microslips is the most important feature. Thus, we conclude that the spatial distributions of microslips contain key information about the stress state of granular gouge and its frictional stability. This study may shed lights on the mechanisms governing earthquake nucleation, microslips, friction fluctuations, and their connection during the stick-slip dynamics of earthquake cycles.

CRediT authorship contribution statement

Gang Ma: Conceptualization, Formal analysis, Investigation, Methodology, Software, Writing – review & editing. **Jiangzhou Mei:** Conceptualization, Data curation, Methodology, Validation, Visualization, Writing – original draft. **Ke Gao:** Formal analysis, Supervision, Validation, Writing – review & editing. **Jidong Zhao:** Validation, Writing – review & editing. **Wei Zhou:** Funding acquisition, Project administration. **Di Wang:** Supervision, Visualization.

Declaration of competing interest

The authors declare that they have no known competing financial interests or personal relationships that could have appeared to influence the work reported in this paper.

Acknowledgements

We acknowledge the financial support from the National Natural Science Foundation of China (Grant No. 51825905, U1865204, and 51779194) and Science project of China Huaneng Group Co. Ltd (HNKJ18-H26). The numerical calculations in this work have been done on the supercomputing system in the Supercomputing Center of Wuhan University. The data supporting this paper can be found at the corresponding author's figshare repository (https://figshare.com/articles/dataset/Machine_learning_bridges_microslips_and_slip_avalanches_of_sheared_granular_gouge/14099417).

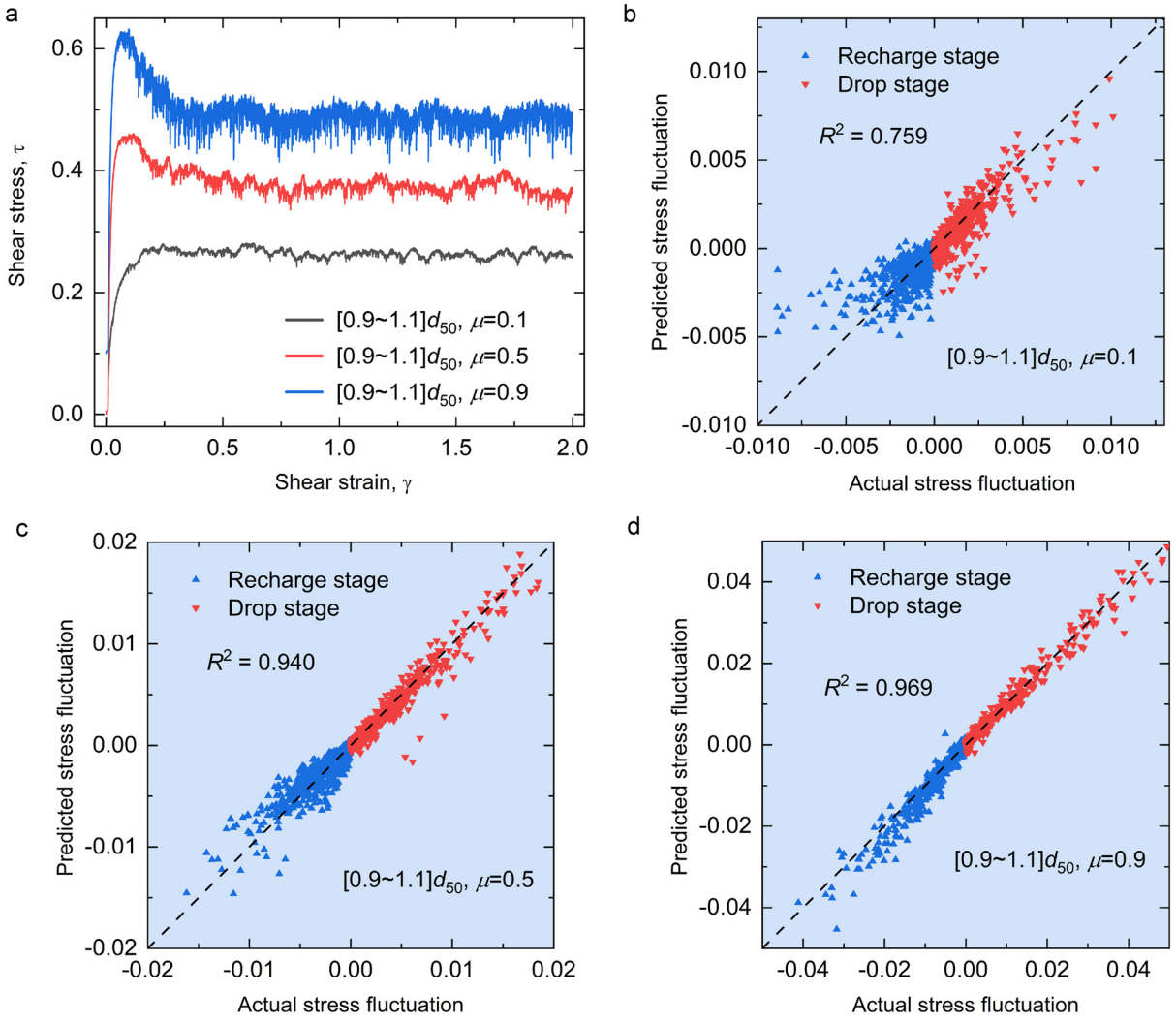

Fig. 10. (a) Stress-strain curves of different particles frictions. The top curve has been shifted vertically by 0.1 to facilitate visual inspection. The prediction performances of XGBoost trained on these datasets are shown from (b) to (d), respectively. Here we only show the results based on MRF.

Appendix A. Nomenclature of symbols for defining features

Table A1
Nomenclature of symbols for defining features.

Symbol	Meaning of the symbol
$D^2_{\min,i}$	The nonaffine displacement of particle i
$\phi_{\max,i}$	The maximum value of particle $D^2_{\min}$ within the neighborhood of particle i
$\phi_{\mathrm{mean},i}$	The mean value of particle $D^2_{\min}$ within the neighborhood of particle i
$\phi_{\mathrm{var},i}$	The variance of particle $D^2_{\min}$ within the neighborhood of particle i
$\phi_{\mathrm{skew},i}$	The skewness of particle $D^2_{\min}$ within the neighborhood of particle i
$\phi_{\mathrm{kuro},i}$	The kurtosis of particle $D^2_{\min}$ within the neighborhood of particle i

References

Anthony, J.L., Marone, C., 2005. Influence of particle characteristics on granular friction. J. Geophys. Res., Solid Earth 110 (8), 1–14. https://doi.org/10.1029/2004JB003399.

Aharonov, E., Sparks, D., 2004. Stick-slip motion in simulated granular layers. J. Geophys. Res., Solid Earth 109 (9), 1–12. https://doi.org/10.1029/2003JB002597.

Barés, J., Wang, D., Wang, D., Bertrand, T., O'Hern, C.S., Behringer, R.P., 2017. Local and global avalanches in a two-dimensional sheared granular medium. Phys. Rev. E 96 (5), 1–13. https://doi.org/10.1103/PhysRevE.96.052902.

Baró, J., Corral, Á., Illa, X., Planes, A., Salje, E.K.H., Schranz, W., et al., 2013. Statistical similarity between the compression of a porous material and earthquakes. Phys. Rev. Lett. 110 (8), 1–5. https://doi.org/10.1103/PhysRevLett.110.088702.

Bolton, D.C., Shreedharan, S., Rivière, J., Marone, C., 2020. Acoustic energy release during the laboratory seismic cycle: insights on laboratory earthquake precursors and prediction. J. Geophys. Res., Solid Earth 125 (8). https://doi.org/10.1029/2019JB018975.

Cao, P., Dahmen, K.A., Kushima, A., Wright, W.J., Park, H.S., Short, M.P., Yip, S., 2018. Nanomechanics of slip avalanches in amorphous plasticity. J. Mech. Phys. Solids 114, 158–171. https://doi.org/10.1016/j.jmps.2018.02.012.

Cao, P., Short, M.P., Yip, S., 2019. Potential energy landscape activations governing plastic flows in glass rheology. Proc. Natl. Acad. Sci. USA 116 (38), 18790–18797. https://doi.org/10.1073/pnas.1907317116.

Chen, T., Guestrin, C., 2016. XGBoost: a scalable tree boosting system. J. Assoc. Phys. India 42 (8), 665.

Chikkadi, V., Schall, P., 2012. Nonaffine measures of particle displacements in sheared colloidal glasses. Phys. Rev. E, Stat. Nonlinear Soft Matter Phys. 85 (3), 1–5. https://doi.org/10.1103/PhysRevE.85.031402.

Cipelletti, L., Martens, K., Ramos, L., 2019. Microscopic precursors of failure in soft matter. Soft Matter 16 (1), 82–93. https://doi.org/10.1039/c9sm01730e.

Corbi, F., Sandri, L., Bedford, J., Funiciello, F., Brizzi, S., Rosenau, M., Lallemand, S., 2019. Machine learning can predict the timing and size of analog earthquakes. Geophys. Res. Lett. 46 (3), 1303–1311. https://doi.org/10.1029/2018GL081251.

Dorostkar, O., Carmeliet, J., 2019. Grain friction controls characteristics of seismic cycle in faults with granular gouge. J. Geophys. Res., Solid Earth 124 (7), 6475–6489. https://doi.org/10.1029/2019JB017374.

Dorostkar, O., Guyer, R.A., Johnson, P.A., Marone, C., Carmeliet, J., 2018. Cohesion-induced stabilization in stick-slip dynamics of weakly wet, sheared granular fault gouge. J. Geophys. Res., Solid Earth 123 (3), 2115–2126. https://doi.org/10.1002/2017JB015171.

Ferdowsi, B., Griffa, M., Guyer, R.A., Johnson, P.A., Marone, C., Carmeliet, J., 2013. Microslips as precursors of large slip events in the stick-slip dynamics of sheared granular layers: a discrete element model analysis. Geophys. Res. Lett. 40 (16), 4194–4198. https://doi.org/10.1002/grl.50813.

Ferdowsi, B., Griffa, M., Guyer, R.A., Johnson, P.A., Carmeliet, J., 2014. Effect of boundary vibration on the frictional behavior of a dense sheared granular layer. Acta Mech. 225 (8), 2227–2237. https://doi.org/10.1007/s00707-014-1136-y.

Friedman, J.H., 2002. Stochastic gradient boosting. Comput. Stat. Data Anal. 38 (4), 367–378. https://doi.org/10.1016/S0167-9473(01)00065-2.

Gao, K., Euser, B.J., Rougier, E., Guyer, R.A., Lei, Z., Knight, E.E., et al., 2018. Modeling of stick-slip behavior in sheared granular fault gouge using the combined finite-discrete element method. J. Geophys. Res., Solid Earth. https://doi.org/10.1029/2018JB015668.

Gao, K., Guyer, R., Rougier, E., Ren, C.X., Johnson, P.A., 2019. From stress chains to acoustic emission. Phys. Rev. Lett. 123 (4). https://doi.org/10.1103/PhysRevLett.123.048003.

Houdoux, D., Amon, A., Marsan, D., Weiss, J., Crassous, J., 2021. Micro-slips in an experimental granular shear band replicate the spatiotemporal characteristics of natural earthquakes. Commun. Earth Environ. 2 (1), 90. https://doi.org/10.1038/s43247-021-00147-1.

Hulbert, C., Rouet-Leduc, B., Johnson, P.A., Ren, C.X., Rivière, J., Bolton, D.C., Marone, C., 2019. Similarity of fast and slow earthquakes illuminated by machine learning. Nat. Geosci. 12 (1), 69–74. https://doi.org/10.1038/s41561-018-0272-8.

Ikari, M.J., Marone, C., Saffer, D.M., 2011. On the relation between fault strength and frictional stability. Geology 39 (1), 83–86. https://doi.org/10.1130/G31416.1.

Johnson, P.A., Ferdowsi, B., Kaproth, B.M., Scuderi, M., Griffa, M., Carmeliet, J., et al., 2013. Acoustic emission and microslip precursors to stick-slip failure in sheared granular material. Geophys. Res. Lett. 40 (21), 5627–5631. https://doi.org/10.1002/2013GL057848.

Kloss, C., Goniva, C., Hager, A., Amberger, S., Pirker, S., 2012. Models, algorithms and validation for opensource DEM and CFD-DEM. Prog. Comput. Fluid Dyn. 12 (2–3), 140–152.

Kou, B., Cao, Y., Li, J., Xia, C., Li, Z., Dong, H., et al., 2018. Translational and rotational dynamical heterogeneities in granular systems. Phys. Rev. Lett. 121 (1), 18002. https://doi.org/10.1103/PhysRevLett.121.018002.

Le Bouil, A., Amon, A., McNamara, S., Crassous, J., 2014. Emergence of cooperativity in plasticity of soft glassy materials. Phys. Rev. Lett. 112 (24), 1–5. https://doi.org/10.1103/PhysRevLett.112.246001.

Lundberg, S.M., Lee, S.I., 2017. A unified approach to interpreting model predictions. Adv. Neural Inf. Process. Syst. 30, 4765–4774.

Ma, G., Regueiro, R.A., Zhou, W., Liu, J., 2019. Spatiotemporal analysis of strain localization in dense granular materials. Acta Geotech. 14 (4), 973–990. https://doi.org/10.1007/s11440-018-0685-y.

Ma, G., Zou, Y., Gao, K., Zhao, J., Zhou, W., 2020. Size polydispersity tunes slip avalanches of granular gouge. Geophys. Res. Lett. 47 (23), 1–9. https://doi.org/10.1029/2020gl090458.

Ma, G., Zou, Y., Chen, Y., Tang, L., Ng, T. tat, Zhou, W., 2021. Spatial correlation and temporal evolution of plastic heterogeneity in sheared granular materials. Powder Technol. https://doi.org/10.1016/j.powtec.2020.09.053.

Mair, K., Frye, K.M., Marone, C., 2002. Influence of grain characteristics on the friction of granular shear zones. J. Geophys. Res., Solid Earth 107 (B10) ECV 4-1-ECV 4-9, https://doir.org/10.1029/2001jb000516.

Marone, C., 1998. The effect of loading rate on static friction and the rate of fault healing during the earthquake cycle. Nature 391 (6662), 69–72. https://doi.org/10.1038/34157.

Marone, C., 2018. Training machines in Earthly ways. Nat. Geosci. 11 (5), 301–302. https://doi.org/10.1038/s41561-018-0117-5.

Mousavi, S.M., Beroza, G.C., 2020. A machine-learning approach for earthquake magnitude estimation. Geophys. Res. Lett. 47 (1), 1–7. https://doi.org/10.1029/2019GL085976.

Murphy, K.A., Dahmen, K.A., Jaeger, H.M., 2019. Transforming mesoscale granular plasticity through particle shape. Phys. Rev. X 9 (1), 11014. https://doi.org/10.1103/PhysRevX.9.011014.

Niemeijer, A., Marone, C., Elsworth, D., 2010. Frictional strength and strain weakening in simulated fault gouge: competition between geometrical weakening and chemical strengthening. J. Geophys. Res., Solid Earth 115 (10), 1–16. https://doi.org/10.1029/2009JB000838.

Rathbun, A.P., Renard, F., Abe, S., 2013. Numerical investigation of the interplay between wall geometry and friction in granular fault gouge. J. Geophys. Res., Solid Earth 118 (3), 878–896. https://doi.org/10.1002/jgrb.50106.

Ren, C.X., Dorostkar, O., Rouet-Leduc, B., Hulbert, C., Strebel, D., Guyer, R.A., et al., 2019. Machine learning reveals the state of intermittent frictional dynamics in a sheared granular fault. Geophys. Res. Lett. 46 (13), 7395–7403. https://doi.org/10.1029/2019GL082706.

Rivière, J., Lv, Z., Johnson, P.A., Marone, C., 2018. Evolution of b-value during the seismic cycle: insights from laboratory experiments on simulated faults. Earth Planet. Sci. Lett. 482, 407–413. https://doi.org/10.1016/j.epsl.2017.11.036.

Rouet-Leduc, B., Hulbert, C., Lubbers, N., Barros, K., Humphreys, C.J., Johnson, P.A., 2017. Machine learning predicts laboratory earthquakes. Geophys. Res. Lett. 44 (18), 9276–9282. https://doi.org/10.1002/2017GL074677.

Rouet-Leduc, B., Hulbert, C., Johnson, P.A., 2019. Continuous chatter of the Cascadia subduction zone revealed by machine learning. Nat. Geosci. 12 (1), 75–79. https://doi.org/10.1038/s41561-018-0274-6.

Scuderi, M.M., Carpenter, B.M., Marone, C., 2014. Physicochemical processes of frictional healing: effects of water on stick-slip stress drop and friction of granular fault gouge. J. Geophys. Res., Solid Earth 119, 4090–4105. https://doi.org/10.1002/2013JB010641.

Scuderi, M.M., Marone, C., Tinti, E., Di Stefano, G., Collettini, C., 2016. Precursory changes in seismic velocity for the spectrum of earthquake failure modes. Nat. Geosci. 9 (9), 695–700. https://doi.org/10.1038/ngeo2775.

Snoek, J., Larochelle, H., Adams, R.P., 2012. Practical Bayesian optimization of machine learning algorithms. In: Proceedings of the 25th International Conference on Neural Information Processing Systems, Vol. 25, pp. 2951–2959.

Song, D., Ng, C.W.W., Choi, C.E., Zhou, G.G.D., Kwan, J.S.H., Koo, R.C.H., 2017. Influence of debris flow solid fraction on rigid barrier impact. Can. Geotech. J. 54 (10), 1421–1434. https://doi.org/10.1139/cgj-2016-0502.

Tordesillas, A., Pucilowski, S., Lin, Q., Peters, J.F., Behringer, R.P., 2016. Granular vortices: identification, characterization and conditions for the localization of deformation. J. Mech. Phys. Solids 90, 215–241. https://doi.org/10.1016/j.jmps.2016.02.032.

Trugman, D.T., Mcbrearty, I.W., Bolton, D.C., Robert, A., Marone, C., Johnson, P.A., 2020. The spatio-temporal evolution of granular microslip precursors to laboratory earthquakes. Geophys. Res. Lett., 1–10. https://doi.org/10.1029/2020GL088404.

von Hippel, P.T., 2005. Mean, median, and skew: correcting a textbook rule. J. Stat. Educ. 13 (2). https://doi.org/10.1080/10691898.2005.11910556.

Wang, D., Carmeliet, J., Zhou, W., Dorostkar, O., 2021. On the effect of grain fragmentation on frictional instabilities in faults with granular gouge. J. Geophys. Res., Solid Earth. https://doi.org/10.1029/2020JB020510.

Xing, Y., Zheng, J., Li, J., Cao, Y., Pan, W., Zhang, J., Wang, Y., 2021. X-ray tomography investigation of cyclically sheared granular materials. Phys. Rev. Lett. 126 (4). https://doi.org/10.1103/PhysRevLett.126.048002.

Zheng, J., Sun, A., Wang, Y., Zhang, J., 2018. Energy fluctuations in slowly sheared granular materials. Phys. Rev. Lett. 121 (24), 248001.